American Mineralogist, Volume 74, pages 384–393, 1989

Microstructures and tetrahedral strip-width order and disorder in Fe-rich minnesotaites

Jung Ho Ahn, Peter R. Buseck
Departments of Geology and Chemistry, Arizona State University, Tempe, Arizona 85287-1404, U.S.A.

Abstract

Fe-rich minnesotaites with Fe/(Fe + Mg) ratios of 0.80 and 0.92 were studied using high-resolution transmission electron microscopy (HRTEM). [010] images show the relative positions of tetrahedra and octahedra in the 2:1 layers and the inverted tetrahedra in the interlayer regions. Minnesotaite having Fe/(Fe + Mg) = 0.92 exhibits electron-diffraction patterns characteristic of a *C*-centered cell, but HRTEM images show that tetrahedral strip widths are severely disordered along the **a** direction. The sample with Fe/(Fe + Mg) = 0.80 contains domains of ordered primitive cells as well as disordered *C*-centered cells. Strips that are three and four tetrahedra wide predominate, but newly discovered strips that are two tetrahedra wide and others that are more than four tetrahedra wide also occur in both specimens. Wide tetrahedral strips are more abundant in the minnesotaite having Fe/(Fe + Mg) = 0.80, and a strip 10 tetrahedra wide was observed. Various β^* values occur; they can be derived by displacement of opposing tetrahedral strips across the octahedral sheet within each layer by $(n/10)\mathbf{a}$ along the **a** axis in the primitive-cell minnesotaite. Local variations of β^* values are also associated with strip-width disorder. Crystal regions having $\beta^* = 64°$ are most abundant, but regions having $\beta^* = 52°$ are also common. The Fe/(Fe + Mg) ratio seems to be important in determining the strip-width disorder as well as the average tetrahedral strip width. Increased strip widths tend toward a talc-like structure, which consists of "infinitely" wide tetrahedral strips.

Introduction

Minnesotaite is one of the most abundant Fe-rich sheet silicates in low-grade metamorphosed iron formations. It was long considered to be an Fe analogue of talc because minnesotaite and talc have similar $d_{(001)}$ values and (Fe + Mg):Si ratios (Gruner, 1944). Detailed structural study of minnesotaite has been difficult because it occurs as fine-grained crystals in mixtures with other minerals. Although single-crystal X-ray study by Guggenheim and Bailey (1982) indicated that minnesotaite shows superlattice reflections, the large size of the unit cell, triclinic symmetry, and lack of untwinned crystals hindered the accurate determination of its structure. However, detailed study with transmission electron microscopy and optical diffraction showed that minnesotaite has a complex modulated structure (Guggenheim and Eggleton, 1986).

The minnesotaite structure is based on a continuous octahedral sheet and opposing tetrahedral strips, with the latter continuous along the **b** axis but modulated along the **a** axis as a result of tetrahedral inversion (Guggenheim and Eggleton, 1986). Inverted tetrahedra in the interlayers form chains continuous along the **b** axis; these tetrahedra are connected to the basal oxygens of adjacent tetrahedral strips. In the ideal structures, crystals contain either strips that are four tetrahedra wide or that are alternately three and four tetrahedra wide (these will be called 4- and 3-strips, respectively); the former have a primitive unit cell (*P* cell), and the latter have a *C*-centered cell (*C* cell) (Guggenheim and Eggleton, 1986). However, disordered minnesotaites are common, and they are the focus of the present study.

High-resolution imaging permits direct observation of the structural modulations and nonperiodic intergrowths of minerals and synthetic materials (e.g., Buseck and Cowley, 1983). In the present study, HRTEM images of Fe-rich minnesotaites were obtained at 400 kV to investigate the details of their modulated structures, placing special emphasis on ordered and disordered features of the tetrahedral strips. In addition, image calculations were performed to facilitate accurate interpretation of the experimental images.

Specimens and electron-microprobe analyses

Our samples are from the Sokoman Iron Formation in the Howells River area, at the western edge of the Labrador Trough, Canada. LIF-183 and LC-160 are from the drill core D.D.H. 1032D and 1039D (report by Fink, 1971, as referenced by Klein and Fink, 1976), sampled at depths of 183 and 160 ft (55.8 and 48.8 m), respectively. The regional geologic setting, stratigraphy, mineralogy, and petrography were described by Klein (1974) and Klein and Fink (1976).

The results of electron-microprobe analyses of minnesotaites from the LIF-183 and LC-160 samples are given in Table 1. Although Guggenheim and Eggleton (1986) showed that minnesotaite has a different structure from

0003–004X/89/0304–0384$02.00

that of talc [the ideal formula of *P*-cell minnesotaite is $(Fe,Mg)_{30}Si_{40}O_{96}(OH)_{28}$ and that of *C*-cell minnesotaite is $(Fe,Mg)_{27}Si_{36}O_{86}(OH)_{26}$], analyses are normalized to 11 oxygens for convenience in comparing with previously reported data. Both minnesotaites show only minor Al, indicating that the tetrahedral cations are almost exclusively Si. LIF-183 minnesotaite contains more Mg than LC-160 minnesotaite. No alkali cations were detected in LIF-183, and LC-160 contains minor Na.

Table 1. Electron-microprobe analyses (wt%) of minnesotaite

	LIF-183	LC-160
SiO_2	51.96	50.66
Al_2O_3	0.27	0.18
FeO*	37.10	41.02
MgO	5.38	2.14
MnO_2	0.09	0.37
TiO_2	0.00	0.00
K_2O	0.00	0.00
Na_2O	0.00	0.03
CaO	0.00	0.00
Total	94.80	94.40
Cations on the basis of 11 oxygens		
Si	3.98	3.99
Al	0.02	0.02
Fe*	2.38	2.71
Mg	0.61	0.25
Mn	0.01	0.02
Ti	0.00	0.00
K	0.00	0.00
Na	0.00	0.00
Ca	0.00	0.00
Total	7.00	6.99
Fe/(Fe + Mg)	79.60	91.55

* All Fe was assumed to be Fe^{2+}.

Experimental details

Ion-milled specimens were prepared from petrographic thin sections following the procedure described by Ahn et al. (1988). The specimens were studied at 400 kV with a JEM 4000EX TEM having a structure resolution limit of 1.7 Å and a spherical aberration coefficient (C_s) of 1.0 mm. The top-entry, double-tilting sample holder is capable of ±15° tilts at the standard specimen height and ±30° at 0.5 mm above the standard specimen height. All bright-field images were obtained using a 40-μm objective aperture and a 150-μm condenser aperture. Images were obtained with minnesotaite [010] parallel to the electron beam.

Image calculations

Calculated [010] images of minnesotaite were obtained using Arizona State University multislice programs. They were used to calculate the Fourier coefficients of the crystal potential for the zero-order Laue zone, and then the multiple electron-scattering calculations were performed. The simulated images were synthesized taking into account experimental conditions.

Because of the lack of a good structure refinement, atomic coordinates of the minnesotaite structure are not available. Approximate (x,y) fractional coordinates of individual atomic sites were determined from the structure model of Guggenheim and Eggleton (1986). The z coordinates of apical oxygens and OH ($z = 0.11$), Si ($z = 0.29$), and basal oxygens ($z = 0.35$) were obtained from their one-dimensional electron-density data. Tetrahedral rings were assumed to be fully extended, thereby allowing the assumption of hexagonal geometry for portions of the structure. Only the *P*-cell structure ($\beta = 127°$) with $P\bar{1}$ symmetry was calculated. Input data included 120 atomic positions, and a total of 194 atomic sites per unit cell were generated by symmetry operations for the image calculation.

TEM results

Image interpretation

The widths and stacking relations of the tetrahedral strips can be determined from images obtained with [010] parallel to the electron beam. For this orientation, the continuous direction of the strips parallels the electron beam. Calculated [010] images at underfocused conditions (−350 to −550 Å) (Fig. 1) show that interlayer regions consist of white bands (I in Fig. 2) elongated along **a** and interrupted by narrow dark bands (D in Fig. 2). These dark bands coincide with the positions of the inverted tetrahedra in the interlayer regions. Inverted tetrahedra connect the tetrahedral strips along the basal planes as well as across the interlayers. The calculated images are consistent with the interpretations of Guggenheim and Eggleton (1986).

For focus between −350 and −550 Å, well-defined rows of white spots (T in Fig. 2) occur on each side of the interlayers (Fig. 1). Additional rows of white spots (O in Fig. 2) occur in the positions of the octahedral sheets. The T spots correspond to channels between the tetrahedrally coordinated cations and so provide information on the widths of the tetrahedral strips. Strips that are four tetrahedra wide yield three such white spots in calculated images of the *P*-cell structure; n white spots indicate the presence of strips having widths of $(n + 1)$ tetrahedra on opposite sides of the octahedral sheets. The number of such spots was used in this study for interpreting the widths of tetrahedral strips.

Ordering and disordering of tetrahedral strips

Although selected-area electron diffraction (SAED) patterns from most grains of LC-160 minnesotaite exhibit the characteristics of a *C* cell, [010] images reveal that the tetrahedral strips are severely disordered (Figs. 3 and 4). The occurrence of ordered 3- and 4-strips [indicated as (34)] is limited to only small portions of crystal (Fig. 5). Although (34) strip sequences occur along the **a** direction, ordering in most grains is not sustained along **c** (Fig. 3). Tetrahedral strip-width disorder occurs as a result of nonperiodic intergrowths of extra 3- and 4-strips, and (33) and (44) units are locally common in disordered *C*-cell minnesotaite (Fig. 4a). Moreover, in such disordered crystals, there are also sequences such as (344) or (3334) (Fig. 4b). The LIF-183 specimen exhibits abundant ordered *P*-cell domains (Fig. 6), although disordered *C*-cell areas are also common.

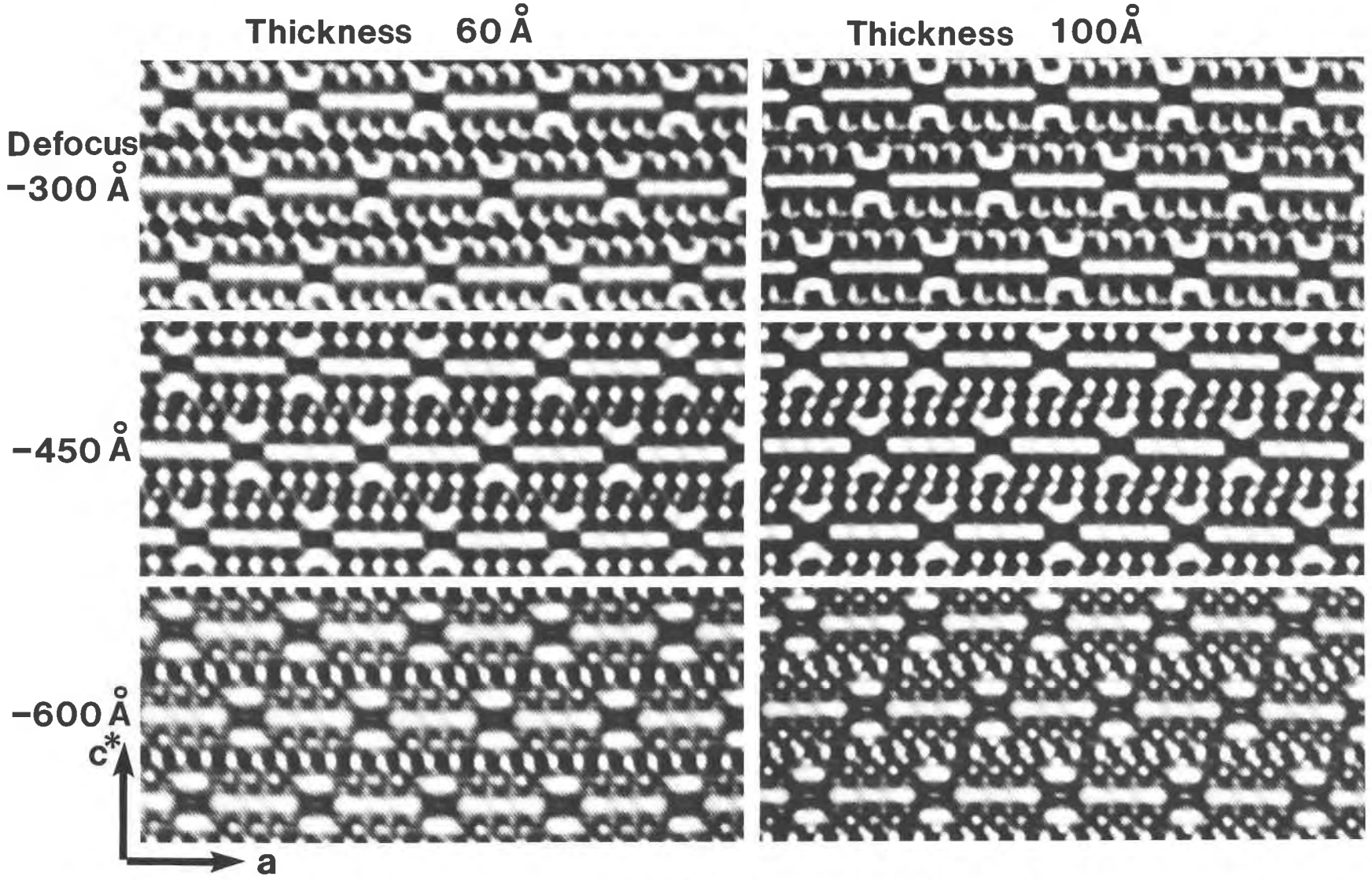

Fig. 1. Calculated [010] images of *P*-cell minnesotaite ($\beta = 127°$) as a function of crystal thickness and defocus. All images were calculated for $C_s = 1.0$ mm, an accelerating voltage of 400 kV, and an objective aperture with radius 0.6 Å^{-1} centered on the incident beam. The optimum defocus condition occurs near −450 Å.

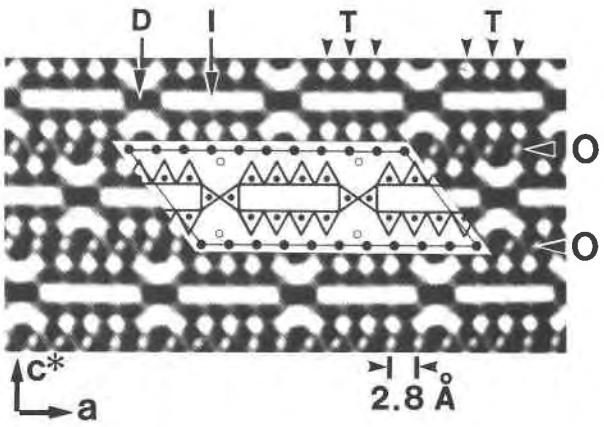

Fig. 2. Calculated [010] images of *P*-cell minnesotaite at 60-Å thickness and −450-Å defocus. Some structural features at the interlayer and 2:1 layer regions can be interpreted by matching the calculated images and the model structure. See the text for the explanation of the various spots and bands at the 2:1 layer region and the interlayer. The inset is equivalent to one unit cell.

HRTEM images also show 2- and 5-strips in LC-160 (Fig. 7). Although strips wider than six tetrahedra were not observed in LC-160, such strips were observed in LC-183, including one that is 10 tetrahedra wide (Fig. 8). Guggenheim and Eggleton (1986) noted strips that are five tetrahedra wide. The use of signal processing on digitized minnesotaite images highlights the regions displaying strip disorder (Buseck et al., 1988).

Variable β^* values

The angle β^* can be measured from the relative positions of inverted tetrahedra between layers in [010] HRTEM images. Guggenheim and Eggleton (1986) reported β^* values of 42, 52, and 64°. β^* values of 64° are dominant in both of our specimens, but 52° values are also common. Even within the same grain, domains with different β^* values occur (Fig. 6). Consistent β^* values are possible only where tetrahedral strips are ordered, and many grains of LIF-183 show regions of ordered *P* cells with a single β^* value (Fig. 6). On the other hand, in LC-160, which is more disordered, areas with unique β^* values are scarce (Figs. 3 and 4). The **c**-axis direction changes within a disordered crystal as a result of strip-width errors. Therefore, the **c*** rather than the **c** direction is indicated in the HRTEM images of disordered minnesotaite.

The [010] SAED patterns of most crystals show that $h0l$ reflections are apparently split where $h \neq 10n$ for the *P*-cell structure and where $h \neq 18n$ for the *C*-cell structure (Figs. 9a, 9b). For the *P* cell, the 10,0,l reflections from regions where $\beta^* = 52°$ overlap the 10,0,$l+1$ reflections where $\beta^* = 64°$; this overlap results from a (1/10)**a** displacement between structures having these different β^* values.

Because the hexagonal rings of adjacent 2:1 layers are superimposed and are connected by inverted tetrahedra at the interlayers, displacement is only possible at the octahedral interface within each layer. There are 10 rows of octahedral cations evident in the [010] projection of the *P* cell, and the distance between adjacent rows of cations equals (1/10)**a** or 2.8 Å (Fig. 2). Minnesotaite with $\beta^* = 64°$ can be derived from minnesotaite with $\beta^* = 52°$ by a +(1/10)**a** displacement of opposing tetrahedral strips across the octahedral sheet within each layer (Fig. 10). Shift of tetrahedral strips by −(1/10)**a** [or +(9/10)**a**] in the $\beta^* = 52°$ structure yields the $\beta^* = 42°$ structure. Ten distinct displacement vectors are possible along the **a**-axis

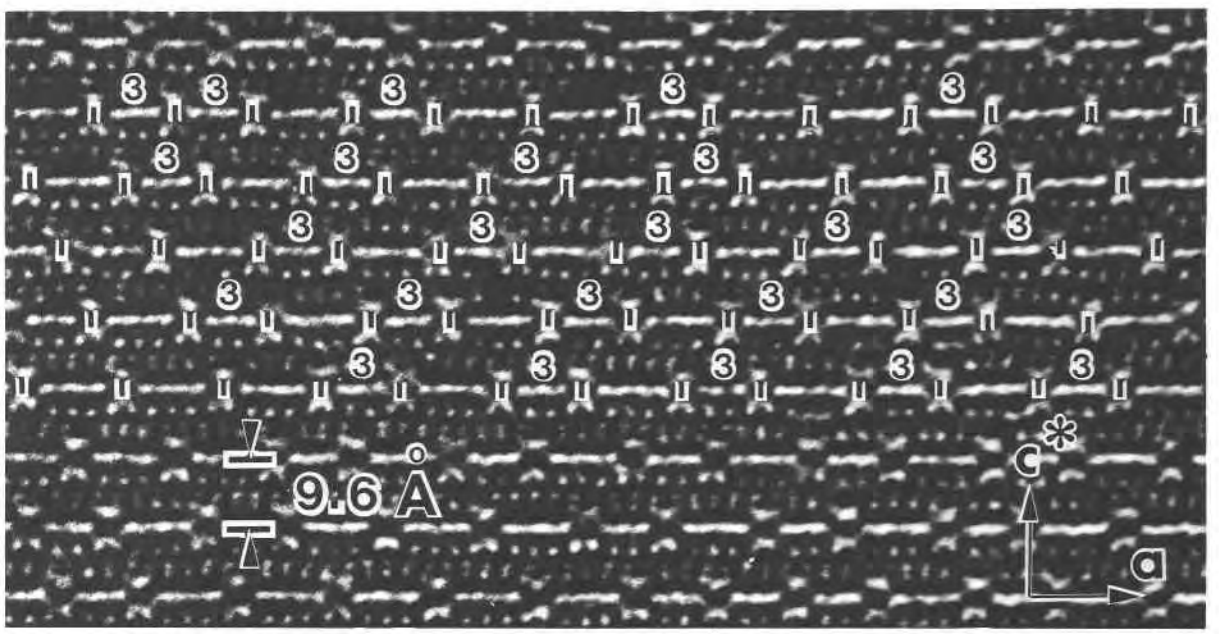

Fig. 3. HRTEM image of disordered *C*-cell minnesotaite from LC-160. The (34) strip sequence is maintained in part of the crystal. The unlabeled strips are four tetrahedra wide.

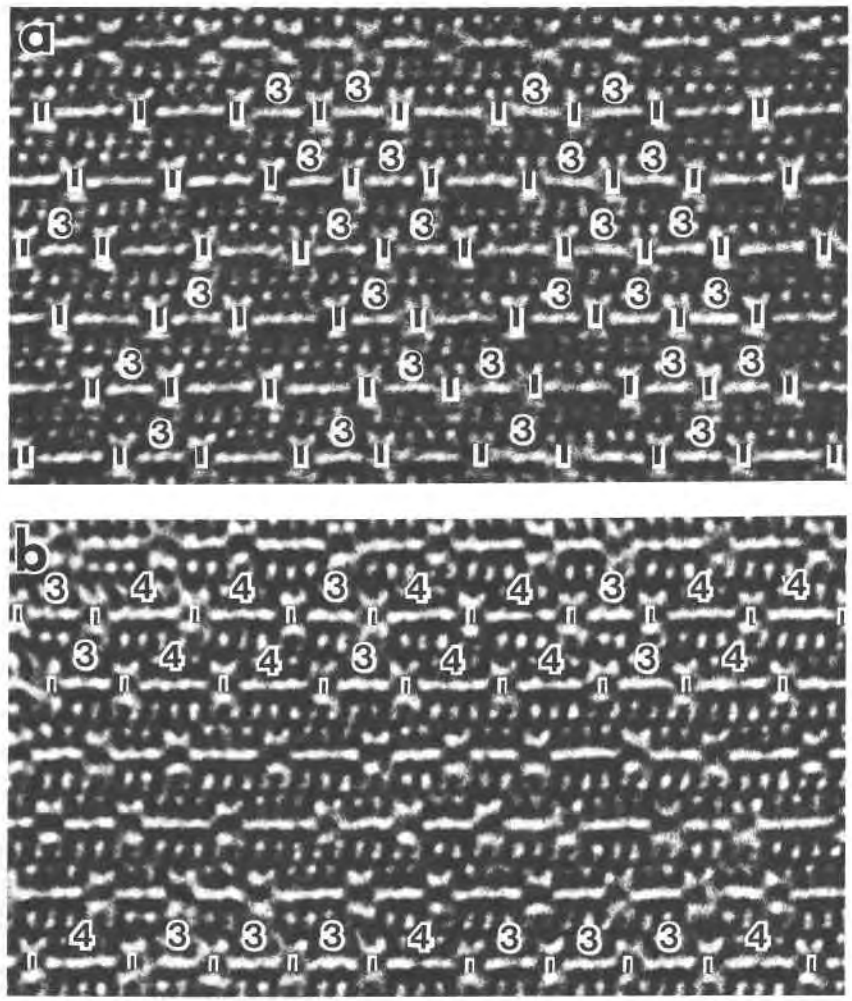

Fig. 4. HRTEM images of disordered minnesotaite from LC-160. (**a**) (33)- and (44)-strip units are common in parts of the crystal, and (**b**) (344)- and (3334)-strip sequences occur locally.

direction for the *P* cell, and eighteen are possible for the *C* cell. Therefore, ten distinct structural forms with different β^* values can be derived from the *P*-cell structure and eighteen from the *C*-cell structure, if intralayer shift along **b** does not occur.

Changes in β^* values also occur where tetrahedral strip-width disorder is present. For example, the intergrowth of 3-strips with *P*-cell material consisting of 4-strips results in the displacement along **a** of the other 4-strips in the same basal plane, and as a consequence, the β^* value

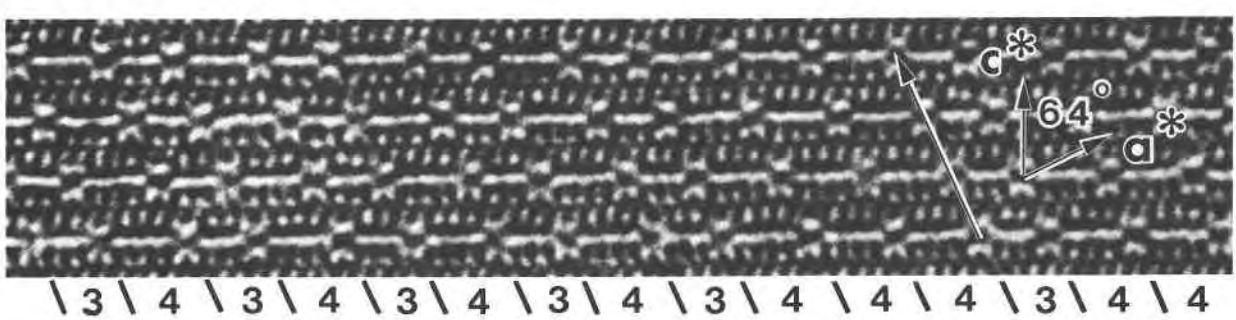

Fig. 5. HRTEM image of a region containing partially ordered *C*-cell minnesotaite from LC-160. Although the tetrahedral-strip sequence deviates from that of the ideal *C* cell, the ordered stacking yields a single β^* angle of 64°.

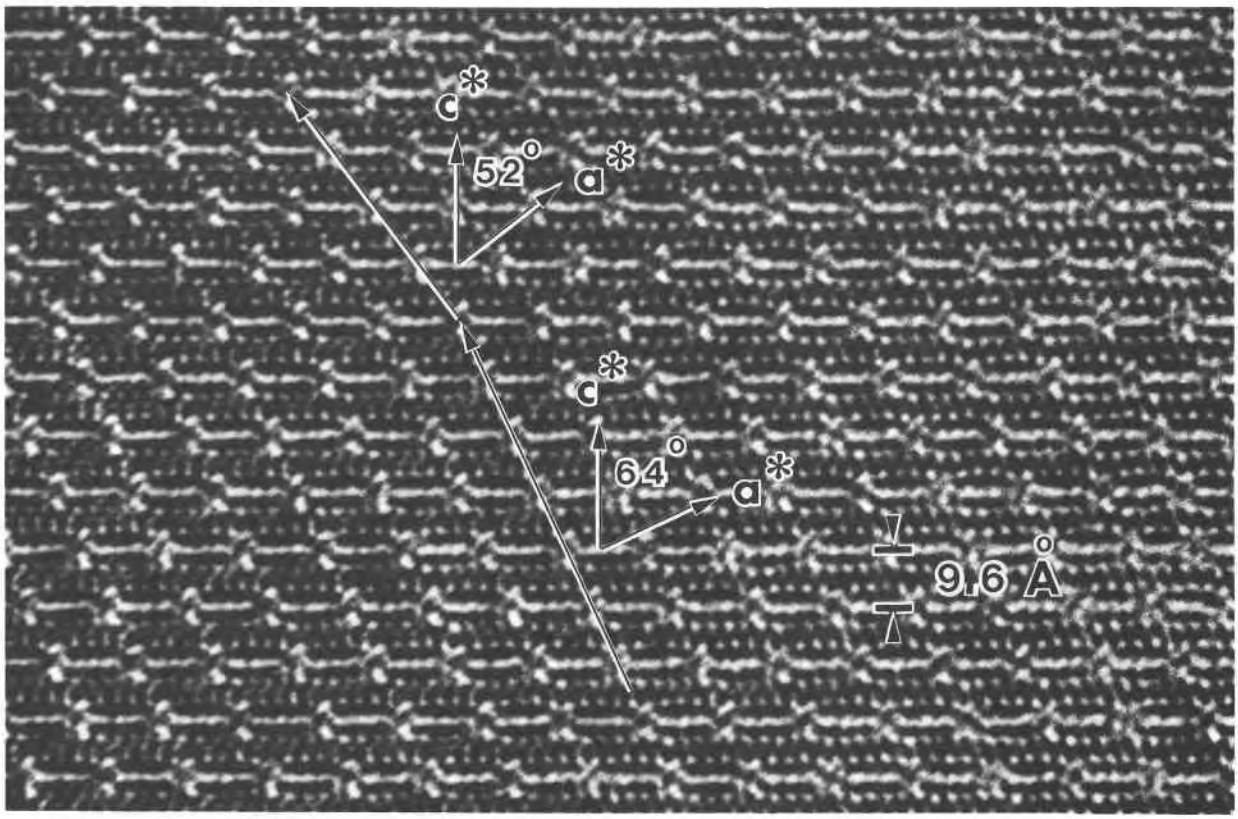

Fig. 6. HRTEM image of ordered *P*-cell minnesotaite from LIF-183. Two different values of β^* occur, and an ordered tetrahedral strip sequence is maintained.

changes in that layer. However, some areas having strip-width disorder show single values of β^* because adjacent layers have the same strip-width sequences along **a** (Fig. 5).

Beam damage of minnesotaite

Many 2:1 layer silicates are known to damage easily in the electron beam (Veblen and Buseck, 1983; Ahn et al., 1986), but minnesotaite is relatively resistant to beam damage. The sharing of inverted tetrahedra by adjacent tetrahedral sheets produces strong bonding at the interlayer and presumably accounts for the enhanced resistance of minnesotaite to electron-beam irradiation. Experience with 120-, 200-, and 400-kV electron microscopes indicates that minnesotaite damages faster in the electron beam at higher acceleration voltages, even though inelastic scattering of electrons decreases with higher voltages (Hobbs, 1979).

Discussion

Minnesotaites having high Fe/(Fe + Mg) ratios are expected to experience greater tetrahedral and octahedral sheet misfit than Mg-rich crystals, provided there are no accompanying chemical changes in the tetrahedral sheets. This predicted misfit (Guggenheim and Eggleton, 1987) results from the larger cation size of Fe^{2+} than Mg^{2+}. Guggenheim and Eggleton (1986) found that the *C*-cell structure predominates in material with Fe/(Fe + Mg) = 0.87 and that minnesotaite having Fe/(Fe + Mg) = 0.64 predominantly has a *P*-cell structure. Our HRTEM data also

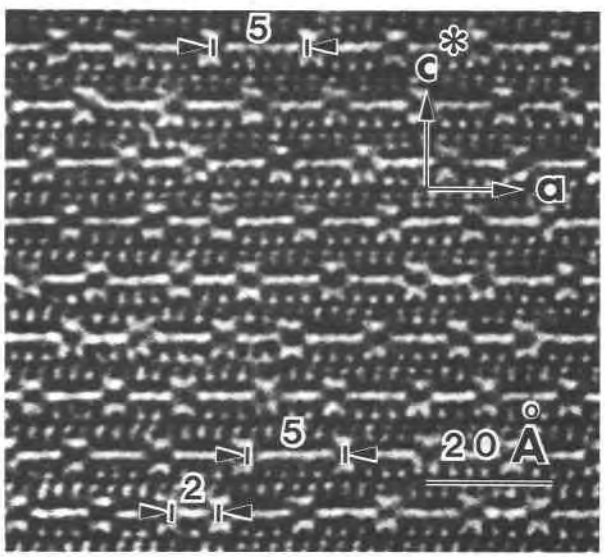

Fig. 7. HRTEM image showing 2- and 5-strips within disordered *C*-cell minnesotaite from LC-160.

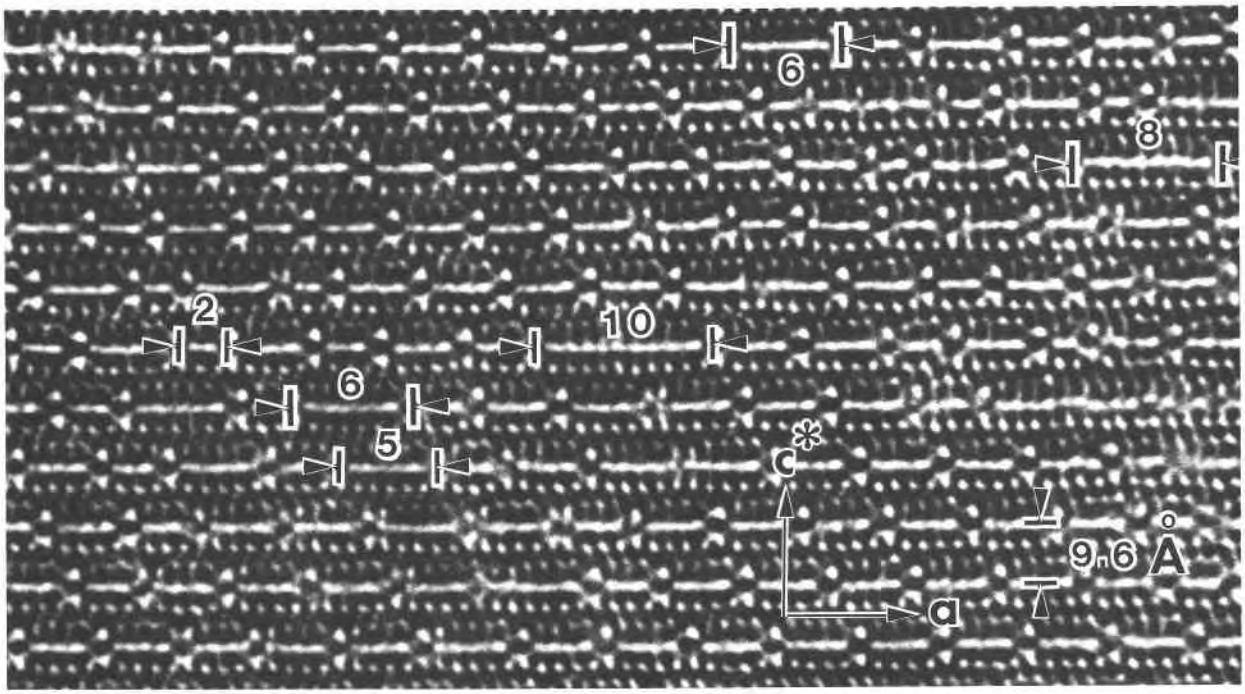

Fig. 8. HRTEM images of minnesotaite from LIF-183 showing strips that are 2-, 5-, 6-, 8-, and 10-tetrahedra wide.

show this trend; more abundant 3-strips occur in LC-160, and wide tetrahedral strips are more abundant in LIF-183.

Analyses of minnesotaites show that it can accommodate a wide range of Fe-Mg substitution (e.g., Klein, 1974; Lesher, 1978; Floran and Papike, 1978; Klein and Gole, 1981; Klein, 1983). A complete range of compositions apparently exists between ideal Fe-rich *P*-cell minnesotaite and Mg-rich *C*-cell minnesotaite, raising a question about the structural discontinuity between *P*- and *C*-cell minnesotaites. The chemistry of the octahedral and tetrahedral sheets determines the degree of sheet misfit (Guggenheim and Eggleton, 1987); if the tetrahedral inversions result from this misfit, then most minnesotaites would have 3- to 4-strip ratios that would produce neither the ordered *P*-cell structures nor the ordered *C*-cell structures. Unless such crystals are segregated into separate domains of ordered *P* and *C* cells, or they form other new ordered structures, disordered tetrahedral strip sequences will result, and they are common. However, the determination of the chemistry of ideal *P*- and *C*-cell structures is difficult or impossible because of the many variables such as substitution of other elements, the oxidation state of Fe, structural distortion, and possible cation ordering.

The limit of Fe-Mg substitution in the talc-minnesotaite series is not known, but "ferroan talc," which is chemically similar to Mg-rich minnesotaite, occurs in some relatively unmetamorphosed iron formations (e.g., Floran and Papike, 1978; Lesher, 1978; Ewers and Morris, 1981; Klein and Gole, 1981; Baker, 1985). The most Mg-rich minnesotaite that was confirmed to have the minnesotaite structure has Fe/(Fe + Mg) = 0.58 (Guggenheim and Eggleton, 1986). The common occurrence of strips wider than four tetrahedra in LC-183 suggests that some Mg-rich minnesotaites (or Fe-rich talcs) could have new longer-period modulated structures consisting of mixtures of 4- and 5-strips or of even wider strips.

Tetrahedral strips having a large range in widths occur in both samples investigated in this study. Increases in tetrahedral strip widths tend toward the talc-like structure, the strips of which can be considered to be "infinite" in width.

The structures projected along [010] show that only one side of the octahedral sheet is coordinated to a tetrahedral sheet in the regions where tetrahedral inversion occurs, resulting in a local 1:1 layer character within minnesotaite (Fig. 9). Guggenheim and Eggleton (1986) suggested that the 1:1 layer character in minnesotaite can allow the octahedral sheet to warp, as it does in antigorite (Kunze, 1956, 1961). Wavelike characteristics of octahedral sheets also occur in other modulated 2:1 layer silicates such as zussmanite (Lopes-Vieira and Zussman, 1969), stilpnomelane (Eggleton, 1972), and ganophyllite (Eggleton and Guggenheim, 1986).

The displacement of opposing tetrahedral strips across the octahedral sheet within each layer changes the relative positions of opposing tetrahedral strips as well as the value of β^*. Shifts of tetrahedral strips by (2/10)**a**, (3/10)**a**, (7/10)**a**, and (8/10)**a** from the $\beta^* = 52°$ structure result in maximum 2:1 layer characteristics because of the approximate superposition of tetrahedral strips across the

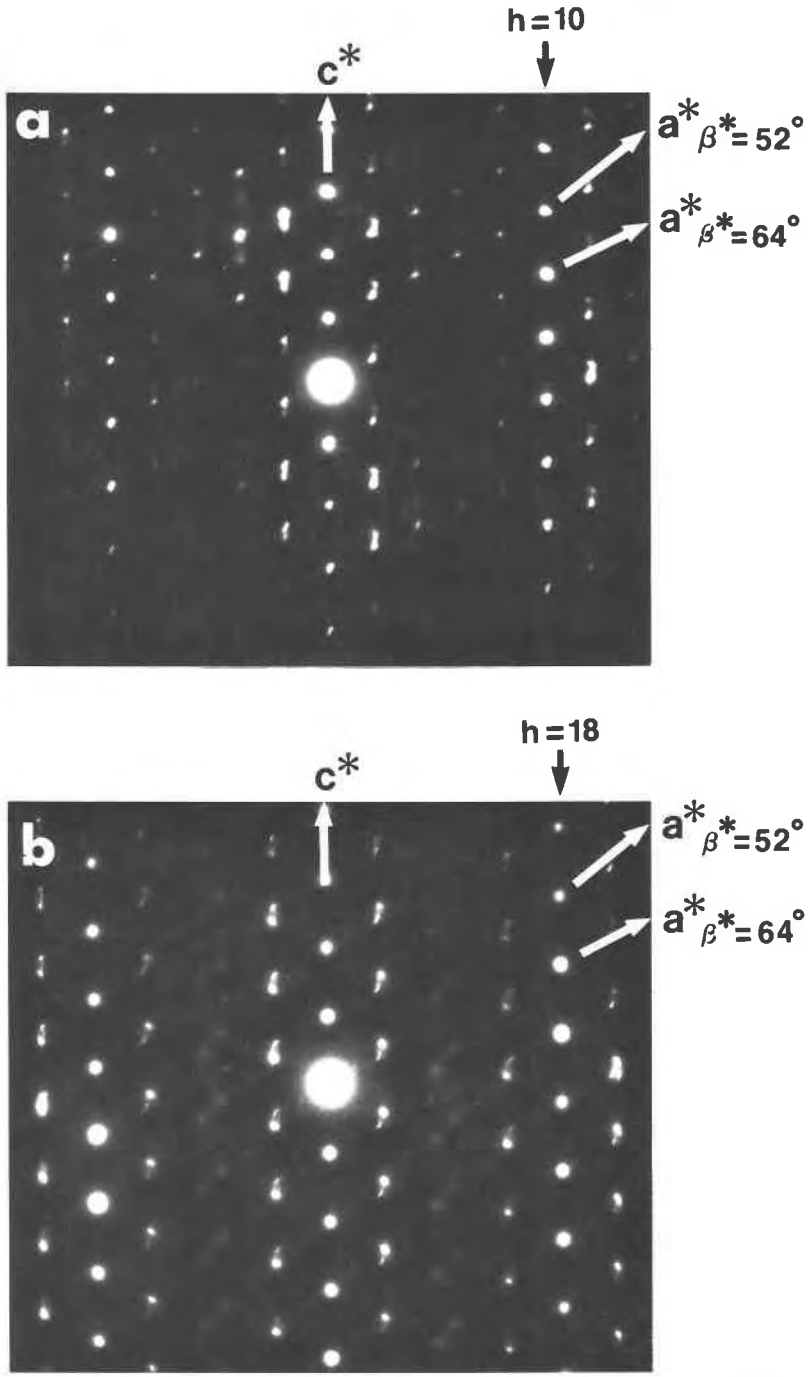

Fig. 9. [010] SAED patterns from (**a**) *P*-cell and (**b**) *C*-cell crystals showing β^* values of 52° and 64°. Reflections with $h \neq 10$ and $h \neq 18$ are apparently split in the *P* and *C* cells, respectively.

octahedral sheet [see Fig. 11a for the structure resulting from a (2/10)**a** displacement]. Neither side of an octahedral sheet is coordinated to the tetrahedral sheets in the regions where tetrahedra are inverted.

Regions of minnesotaite having both opposing tetrahedral strips superimposed across the octahedral sheet were not observed in the present investigation. Regions having $\beta^* = 64°$ are most abundant in both samples investigated in this study, whereas material having $\beta^* = 52°$ is more abundant in the samples studied by Guggenheim and Eggleton (1986). Among possible polymorphs with different β^* angles, the $\beta^* = 64°$ and 52° structures maintain maximum 1:1 layer characteristics (see Fig. 11b for the $\beta^* = 64°$ structure).

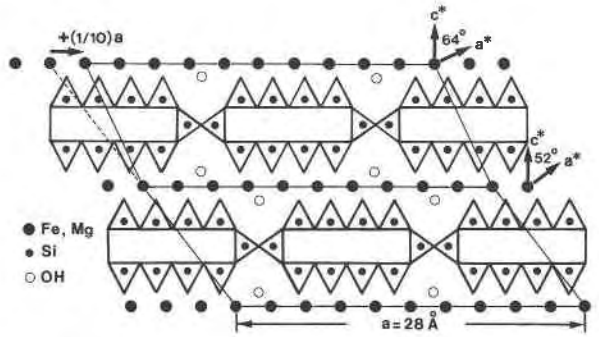

Fig. 10. Schematic illustration of the *P*-cell minnesotaite structure. Displacement of tetrahedral strips across the octahedral sheet by (1/10)**a** from the $\beta^* = 52°$ structure results in the $\beta^* = 64°$ structure. Possible tilting of tetrahedra and warping of octahedral sheets are not considered in this figure (modified after Guggenheim and Eggleton, 1986).

Conclusions

The present HRTEM study indicates that the minnesotaite grains that we investigated have highly disordered strip structures and variable β^* values at the unit-cell scale. The calculated images of minnesotaite are consistent with the experimental images, suggesting that current HRTEM data support the structural model of Guggenheim and Eggleton (1986). In addition to 3- and 4-strips constituting P and C cells, tetrahedral strips having other widths also occur. Minnesotaite structures with various β^* values can be derived by the displacements of tetrahedral strips by $(n/10)$**a** across the octahedral sheet within each layer. Such displacements also change the 2:1 structural characteristics within the layer. Minnesotaite structures with $\beta^* = 64°$ are most abundant, but structures with $\beta^* = 52°$ are also common.

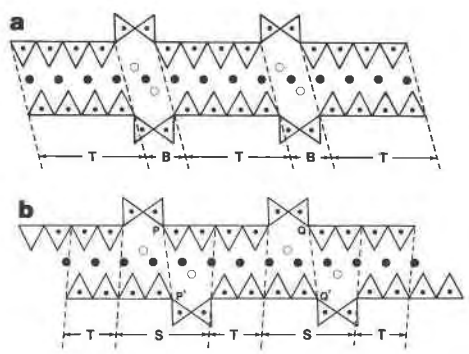

Fig. 11. Idealized *P*-cell minnesotaite structures viewed parallel to the tetrahedral strips (**b** axis). (**a**) The displacement of tetrahedral strips by (2/10)**a** from the $\beta^* = 52°$ structure results in a structure that shows maximum 2:1 layer characteristics. B indicates the part of the octahedral sheet that is not coordinated to tetrahedral strips on either side and so does not exhibit 2:1 layer characteristics. (**b**) The structure having $\beta^* = 64°$ contains two types of regions in the octahedral sheets. The octahedral sheets are coordinated to tetrahedral strips on both sides (T) or only on one side (S). P–P′ and Q–Q′ indicate the areas of inversion, which are locally similar to those of antigorite.

Acknowledgments

We thank J. C. Barry for help with sample preparation and electron microscopy. We are grateful to S. Guggenheim for valuable suggestions and preprints. We thank C. Klein for providing samples and information about them. We also thank J. C. Clark for microprobe analysis. Reviews by S. Guggenheim, D. R. Veblen, and R. J. Reeder improved the manuscript. Electron microscopy was performed at the Facility for High Resolution Electron Microscopy at Arizona State University. The ASU HREM facility is supported by NSF and ASU, and this study was supported by NSF grants EAR 8408168 and EAR 8708529. The electron microprobe used was obtained through NSF grant EAR 8408167.

References cited

Ahn, J.H., Peacor, D.R., and Essene, E.J. (1986) Cation-diffusion–induced characteristic beam damage in transmission electron microscope images of micas. Ultramicroscopy, 19, 375–382.

Ahn, J.H., Burt, D.M., and Buseck, P.R. (1988) Alteration of andalusite to sheet silicates in a pegmatite. American Mineralogist, 73, 559–567.

Baker, J.H. (1985) Greenalite, Mg-rich minnesotaite and stilpnomelane from Ösjöberg and Sirsjöberg iron-ore mines, Hjulsjö, W. Bergslagen, Sweden. Mineralogical Magazine, 49, 611–613.

Buseck, P.R., and Cowley, J.M. (1983) Modulated and intergrowth structures in minerals and electron microscope methods for their study. American Mineralogist, 68, 18–40.

Buseck, P.R., Epelboin, Y., and Rimsky, A. (1988) Signal processing of high-resolution transmission electron microscope images using Fourier transforms. Acta Crystallographica A44, 975–986.

Eggleton, R.A. (1972) The crystal structure of stilpnomelane: II. The full cell. Mineralogical Magazine, 38, 693–711.

Eggleton, R.A. and Guggenheim, S. (1986) A re-examination of the structure of ganophyllite. Mineralogical Magazine, 50, 307–315.

Ewers, W.E., and Morris, R.C. (1981) Studies of the Dale Gorge Member of the Brockman Iron Formation, Western Australia. Economic Geology, 76, 1929–1953.

Floran, R.J., and Papike, J.J. (1978) Mineralogy and petrology of the Gunflint Iron Formation, Minnesota-Ontario: Correlation of compositional and assemblage variations at low to moderate grade. Journal of Petrology, 19, 215–288.

Gruner, J.W. (1944) The composition and structure of minnesotaite, a common iron silicate in iron formations. American Mineralogist, 29, 363–372.

Guggenheim, S., and Bailey, S.W. (1982) The superlattice of minnesotaite. Canadian Mineralogist, 20, 579–584.

Guggenheim, S., and Eggleton, R.A. (1986) Structural modulation in iron-rich and magnesium-rich minnesotaite. Canadian Mineralogist, 24, 479–497.

——— (1987) Modulated 2:1 layer silicates: Review, systematics, and predictions. American Mineralogist, 72, 724–738.

Hobbs, L.W. (1979) Radiation effects in analysis of inorganic specimens by TEM. In J.J. Hren, J.I. Goldstein, and D.C. Joy, Eds., Introduction to analytical electron microscopy, p. 437–480. Plenum Press, New York.

Klein, C., Jr. (1974) Greenalite, stilpnomelane, minnesotaite, crocidolite and carbonates in a very low-grade metamorphic Precambrian iron-formation. Canadian Mineralogist, 12, 475–498.

——— (1983) Diagenesis and metamorphism of Precambrian banded iron-formations. In A.F. Trendall and R.C. Morris, Eds., Iron-formation: Facts and problems, p. 417–469. Elsevier, Amsterdam.

Klein, C., Jr., and Fink, R.P. (1976) Petrology of the Sokoman Iron Formation in the Howells River area, at the western edge of the Labrador Trough. Economic Geology, 71, 453–487.

Klein, C., Jr., and Gole, M.J. (1981) Mineralogy and petrology of the Marra Mamba Iron Formation, Hamersley Basin, Western Australia. American Mineralogist, 66, 507–525.

Kunze, G. (1956) Die gewellte Struktur des Antigorits. I. Zeitschrift für Kristallographie, 108, 82–107.

——— (1961) Antigorit. Strukturtheoretische Grundlagen und ihre prak-

tische Bedeutung für weitere Serpentin-Forschung. Fortschritte der Mineralogie, 39, 206–324.

Lesher, C.M. (1978) Mineralogy and petrology of the Sokoman Iron Formation near Ardua Lake, Quebec. Canadian Journal of Earth Sciences, 15, 480–500.

Lopes-Vieira, A., and Zussman, J. (1969) Further detail on the crystal structure of zussmanite. Mineralogical Magazine, 37, 49–60.

Veblen, D.R., and Buseck, P.R. (1983) Radiation effects on minerals in the electron microscope. In G.W. Bailey, Ed., Proceedings of the 41st Annual Meeting of the Electron Microscopy Society of America, p. 350–353. San Francisco Press, San Francisco.

Manuscript received February 11, 1988
Manuscript accepted October 3, 1988